Synthesis and Mesomorphism of Related Series of Triphilic Ionic Liquid Crystals based on 1,2,4-Triazolium Cations

Alessio Riccobono,[a,b] Giuseppe Lazzara,[c] Sarah E. Rogers,[d] Ivana Pibiri*[,b] Andrea Pace,[b] John M. Slattery[a] and Duncan W. Bruce*[,a]

[a] Department of Chemistry
University of York
Heslington
YORK YO10 5DD (UK)
Tel: (+44) 1904 324085
E-mail: duncan.bruce@york.ac.uk

[b] Dipartimento di Scienze e Tecnologie Biologiche,
Chimiche e Farmaceutiche e Tecnologie,
Ed. 17 Viale delle Scienze,
90128 Palermo,
ITALY
E-mail: ivana.pibiri@unipa.it

[c] Dipartimento di Chimica e Fisica,
Università Degli Studi di Palermo,
Ed. 17 Viale delle Scienze,
90128 Palermo,
ITALY

[d] ISIS,
Science & Technology Facilities Council,
Rutherford Appleton Laboratory,
Didcot,
OX11 0QX,
UK

Abstract:

The synthesis, liquid crystal and conductivity properties of a series of 27 salts based on the 5-(4-(alkyloxy)phenyl)-1,2,4-triazol-4-ium cation bearing a perfluoroalkyl chain with triflate, tetrafluoroborate and bistriflimide anion are reported. The cations are regarded as triphilic on account of their three distinct regions – hydrocarbon, fluorocarbon and ionic. The mesophases were characterised by a combination of polarised optical microscopy, calorimetry and small-angle scattering experiments using both X-rays and neutrons, while thermal stability was probed using thermogravimetric analysis. The liquid-crystal properties are found to be dependent on the anion and the length of the perfluorocarbon chain, which effects combine to determine aspects of the self-organisation in the mesophases. A strong dependence of conductivity on the anion is seen, which is in turn related to the charge density of the anion.

Graphic Abstract:

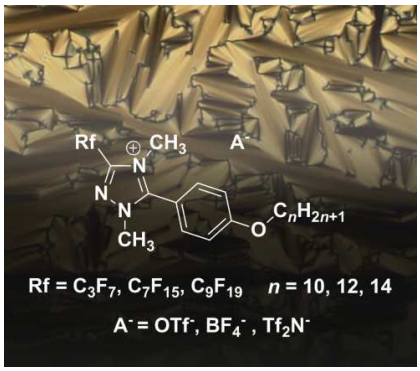

Introduction

Ionic liquids (ILs) have, in recent years, been developed for a diverse range of applications including as reaction media in catalysis,[1–9] removal of mercury from natural gas,[10] as electrolytes in energy applications,[11–26] in the synthesis of nanomaterials,[27–32] for carbon capture and storage[33–36] and many more.[37,38] Liquid crystals (LCs) represent a state of matter intermediate between solids and liquids and are most notably used in low-power, flat-panel displays and other technological devices.[39–41] Ionic liquid crystals (ILCs) therefore combine the favourable properties of ILs with the anisotropic ordering in LCs to produce materials that are often found to have large mesophase ranges, are intrinsically conducting, have high chemical and thermal stabilities and can dissolve a range of solutes.[39,40,42,43] As such, they provide interesting opportunities for exploitation and example have been reported of their application as electrolytes for batteries,[44] as electrochemical sensors [45,46] and as dye-sensitised solar cells,[47] as well as in membranes for water desalination,[48] fuel cells,[49] and extraction processes as solvents.[39] ILCs can also be used to immobilise transition-metal catalysts in the liquid phase of biphasic catalytic reactions[39] or as alternative solvents for various organic reactions, with benefits of an enhancement of the selectivity, yield or activity of catalytic reactions.[50–52]

In calamitic (rod-like) materials, the liquid-crystalline behaviour is dominated by the formation of the SmA phase, with an accompanying SmB phase being observed on some occasions.[53–56] In general, the anisotropic ion tends to be the cation with relatively small anions such as BF_4^-, PF_6^-, OTf^- and halide, although there are examples with tetrachlorometallates.[55,57,58] Liquid-crystalline behaviour is, however, much less commonly observed where the anion is bistriflimide,[59–63] although this may have more to do with the nature of the cation with which it is used, so that it can be expected that liquid crystal phases would be more common with larger, more anisotropic anions.

Fluorine-containing ILs have been the subject of great interest in recent years due to the wide range of properties, such as viscosity, melting point, density, conductivity, solubility, liquid range,

thermal and hydrolytic stability, that can be tuned by modifying the fluorine-content of the cation or the anion.[64,65] Fluorinated moieties can also provide peculiar properties to the materials such as the enhanced ability for gas sorption.[66,67] Over the past decade, the properties of small fluorinated or perfluorinated systems based on heteroaromatic rings have been studied and new fluorinated ILs,[66,68,69] protic ILs,[70] ILCs,[68,69,71,72] and ILCs based on halogen bonding[73] have been discovered. In other cases LC properties have been obtained by replacing an alkyl-chain with a fluorinated chain.[74] The perfluoroalkyl chain is instrumental in influencing the mesomorphism and the tendency for alkyl and perfluoroalkyl chains to segregate from one another leads to a predominance of smectic phases.[68,71,72]

Previously, we reported the mesomorphism of a small family of six 1,2,4-triazolium triflates with C_{10}, C_{12} or C_{14} alkoxy chains and perfluoropropyl or perfluoroheptyl chains.[75] We now report the results of a much wider study that includes materials with a perfluorononyl chain and the anions BF_4^-, Tf_2N^- to give a series of 27 salts. These have been characterised extensively allowing a much greater insight into the relationships between structure and function, as is now described. Families of unsymmetric 1,2,3-triazolium salts [76–78] were reported a few years ago and showed complex polymorphism in some cases although the assignment of mesophases was not always complete.

Results and Discussion

Synthesis

A key step in the synthetic route to these fluorinated triazolium salts, is the preparation of the 3-perfluoroalkyltriazole **4** by ANRORC-like rearrangements[69,75,79–81] starting from the corresponding 5-perfluoroalkyloxadiazole **3**, obtained *via* the conventional amidoxime route (Scheme 1).[82,83]

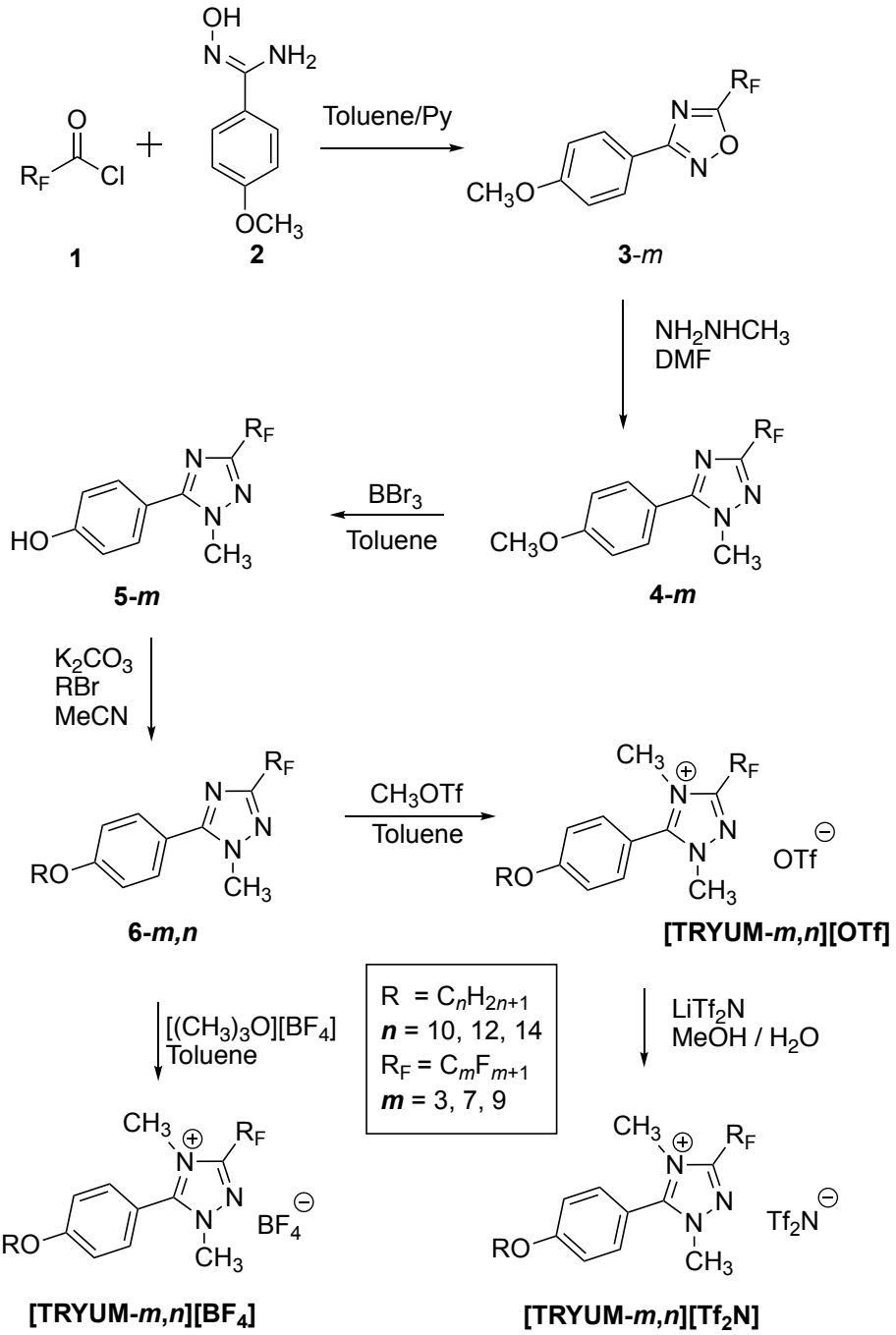

Scheme 1. General synthetic pathways to the target salts.

The methylation of triazoles **6-*m,n*** with MeOTf afforded the triflate salts **[TRYUM-*m,n*][OTf]** salts and metathesis of these using $LiTf_2N$ in methanol, followed by precipitation with water, led to the triflimide salts **[TRYUM-*m,n*][Tf_2N]**. However, preparation of the tetrafluoroborate salts **[TRYUM-*m,n*][BF_4]** was best realized by methylation of **6-*m,n*** using trimethyloxonium tetrafluoroborate. It is worth noting that if ethyl acetate was used as solvent in these methylation reactions, a 10:1 mixture of *N*-methylated and *N*-ethylated product was obtained. Although not investigated in detail, it is likely that the $[Me_3O]^+$ cation methylates EtOAc to give the $[(Et)(Me)(AcO)O]^+$ cation, which can act as a methylating or ethylating agent (see ESI, section 1, for full details). As such, the use of toluene or dichloromethane as solvent allowed us to obtain only the desired *N*-methylated products.

The regiospecificity of the methylation site was confirmed by HMBC and nOe NMR analysis and is in agreement with previous findings.[54,55] Specifically, hydrogens of the N(4)-methyl group couple with both C(3) (3.82, 142.55 ppm) and C(5) (3.82, 155.62 ppm) in ^1H-^{13}C HMBC-NMR spectra, as expected for the 1,4-dimethyl-1,2,4-triazol-2-ium regioisomer. Further details of the NMR experiments are found in the ESI, section 2 (Figures S5 and S6). These conclusions were confirmed by the X-ray single crystal structure of **[TRYUM,7,10][OTf]**.[75]

Liquid Crystal Properties

Mesomorphism

The LC properties of the triazolium salts were characterised using a combination of polarised optical microscopy and DSC. The thermal data are listed in Table 1, while the transition temperatures are plotted in Figure 1. Thermogravimetric analysis showed a single mass loss step for all samples between 290 °C and 340 °C, with the residual mass always less than 5%, indicating quantitative decomposition at higher temperature. The onset temperature values for the volatilisation indicate that the $[BF_4]^-$ salts are the most stable towards thermal decomposition

over limited timescales, (See TGA Analysis in ESI Table S1), although long-term thermal stability tests at lower temperatures were not conducted.

Table 1. Transition temperatures and enthalpies obtained from the DSC traces

Compound[a]	Transition[b]	*T* (°C)	Δ*H* (kJ mol^{-1})
[TRYUM-3,10][OTf]	Cr - Cr' Cr'-Iso	60.0 101.7	7.1 21.0
[TRYUM-3,12][OTf]	Cr-Iso	91.3	48.4
[TRYUM-3,14][OTf]	Cr-Iso	73.8	38.5
[TRYUM-7,10][OTf]	Cr-SmA SmA-Iso	105.6 160.8	11.5 5.2
[TRYUM-7,12][OTf]	Cr-SmA SmA-Iso	60.3 163.5	35.8 4.9
[TRYUM-7,14][OTf]	Cr-SmA SmA-Iso	52.0 166.8	19.8 5.2
[TRYUM-9,10][OTf]	Cr-SmA SmA-Iso	48.6 184.3	1.5 5.7
[TRYUM-9,12][OTf]	Cr-SmA SmA-Iso	60.0 196.0	7.0 6.8
[TRYUM-9,14][OTf]	Cr-SmA SmA-Iso	69.2 205.2	13.1 8.1
[TRYUM-3,10][Tf_2N]	Cr-Iso	73.1	36.7
[TRYUM-3,12][Tf_2N]	Cr-Iso	76.5	54.5
[TRYUM-3,14][Tf_2N]	Cr-Iso	81.1	55.4
[TRYUM-7,10][Tf_2N]	Cr-Iso (Iso-SmA)	83.9 (49.6)	40.1 (−2.7)
[TRYUM-7,12][Tf_2N]	Cr'-Cr Cr-Iso (Iso-SmA)	54.9 86.0 (72.6)	5.2 40 (−3.2)
[TRYUM-7,14][Tf_2N]	Cr'-Cr Cr-Iso (Iso-SmA)	78.7 93.4 (91.5)	10.9 48.0 (−4.6)
[TRYUM-9,10][Tf_2N]	Cr-Iso (Iso-SmA)	97.0 (96.8)	41.4 (−3.8)
[TRYUM-9,12][Tf_2N]	Cr-SmA SmA-Iso	97.4 115.5	44.3 4.9
[TRYUM-9,14][Tf_2N]	Cr-SmA SmA-Iso	98.9 133.2	47.8 5.7

[TRYUM-3,10][BF_4]	Cr-Cr'	49.1	22.9
	Cr'-Iso	84.1	4.4
[TRYUM-3,12][BF_4]	Cr-Cr'	65.0	18.6
	Cr'-Iso	88.8	1.3
[TRYUM-3,14][BF_4]	Cr-Cr'	76.2	33.1
	Cr'-Iso	96.4	2.5
[TRYUM-7,10][BF_4]	Cr-Cr'	67.4	20.5
	Cr'-SmB	106.6	7.6
	SmB-SmA	175.9	2.1
	SmA-Iso	233.4	5.3
[TRYUM-7,12][BF_4]	Cr-Cr'	78.7	23.2
	Cr-'SmB	115.1	7.1
	SmB-SmA	169.5	1.7
	SmA-Iso	236.6	5.0
[TRYUM-7,14][BF_4]	Cr-Cr’	63.6	17.4
	Cr’-Cr''	88.7	29.2
	Cr''-SmB	125.2	8.6
	SmB-SmA	175.5	2.0
	SmA-Iso	237.3	5.1
[TRYUM-9,10][BF_4]	Cr-Cr'	73.2	27.9
	Cr'-SmB	115.9	2.1
	SmB-SmA	139.3	9.4
	SmA-Iso	265.6	2.6
[TRYUM-9,12][BF_4]	Cr-Cr'	89.4	22.5
	Cr'-SmB	116.7	5.0
	SmB-SmA	136.8	7.8
	SmA-Iso	268.5	1.0
[TRYUM-9,14][BF_4]	Cr-Cr’	74.7	33.0
	Cr’-Cr''	92.6	13.2
	Cr''-SmB	116.8	3.5
	SmB-SmA	135.5	7.8
	SmA-Iso	257.7	1.3

[a] The first six entries in the table were first reported in the previous communication.[75] [b] Transitions refer to the 1st heating cycles. Data in brackets refer to monotropic transitions.

To understand the behaviour of these compounds, data are first considered for salts of each anion and then a broader comparison is made. Looking first at the BF_4^- salts, none of the materials with a perfluoropropyl chain show LC properties, although there is a steady increase in the melting point from 84.1 °C (**[TRYUM-3,10][BF_4]**) to 96.4 °C (**[TRYUM-3,14][BF_4]**) with increasing alkoxy chain length. On the other hand, by increasing the perfluoroalkyl chain length to seven carbons (C_7F_{15}–), the melting points continue to increase with alkoxy chain length and LC mesophases are observed. The phases are identified readily by optical microscopy as a SmA phase, below which is

a SmB phase. Figure 2 shows clearly the optical texture of the two phases for **[TRYUM-7,10][BF_4]** with the classic focal conic fan texture of the SmA phase formed from the coalescence of bâtonnets,[61] while the SmB phase is differentiated by the appearance of striations across the back of the fans as additional order grows in. With the perfluoroheptyl chain, the SmB phase persists to around 175 °C before giving way to the SmA, which remains until clearing at about 235 °C with very little dependence on alkoxy chain length. However, when compounds with a perfluorononyl chain are considered, the melting point is all but independent of chain length and the SmB phase is destabilised, now clearing around 136-139 °C across the three alkoxy chain lengths. Conversely, the SmA phase is significantly stabilised with clearing points between 258 and 269 °C.

Considering now the triflate salts, as reported previously,[75] those with a perfluoropropyl chain are not liquid crystals but unlike the analogous BF_4^- salts, the melting point decreases with increasing alkoxy chain length. All of **[TRYUM-7*,n*][OTf]** and **[TRYUM-9*,n*][OTf]** show a single liquid crystal phase, namely SmA. For **[TRYUM-7*,n*][OTf]** the melting point decreases with *n* while the clearing point increases so that the mesophase range increases from 55 °C (*n* = 10) to 115 °C (*n* = 14). However, for **[TRYUM-9*,n*][OTf]**, both the melting and the clearing point increase with *n*, giving a mesophase range (136 °C) that is essentially invariant with alkoxy chain length.

It is often held to be the case that bistriflimide salts tend not to have liquid crystal properties,[40] but whereas this is true where the central ring structure (*e.g.* imidazolium systems) is small, where it is more developed then mesophases can be seen.[62,84–86] Thus, in common with the triflate and tetrafluoroborate salts, none of **[TRYUM-3*,n*][Tf_2N]** is mesomorphic, but all of **[TRYUM-7*,n*][Tf_2N]** and **[TRYUM-9*,n*][Tf_2N]** show a SmA phase. In both series, the clearing point increases with alkoxy chain length, as does the melting point but more modestly. For all of **[TRYUM-7*,n*][Tf_2N]** the SmA phase is monotropic (only just for **[TRYUM-7,14][Tf_2N]**), while it is monotropic for **[TRYUM-9,10][Tf_2N]** and enantiotropic for **[TRYUM-9,12][Tf_2N]** and **[TRYUM-9,14][Tf_2N]**.

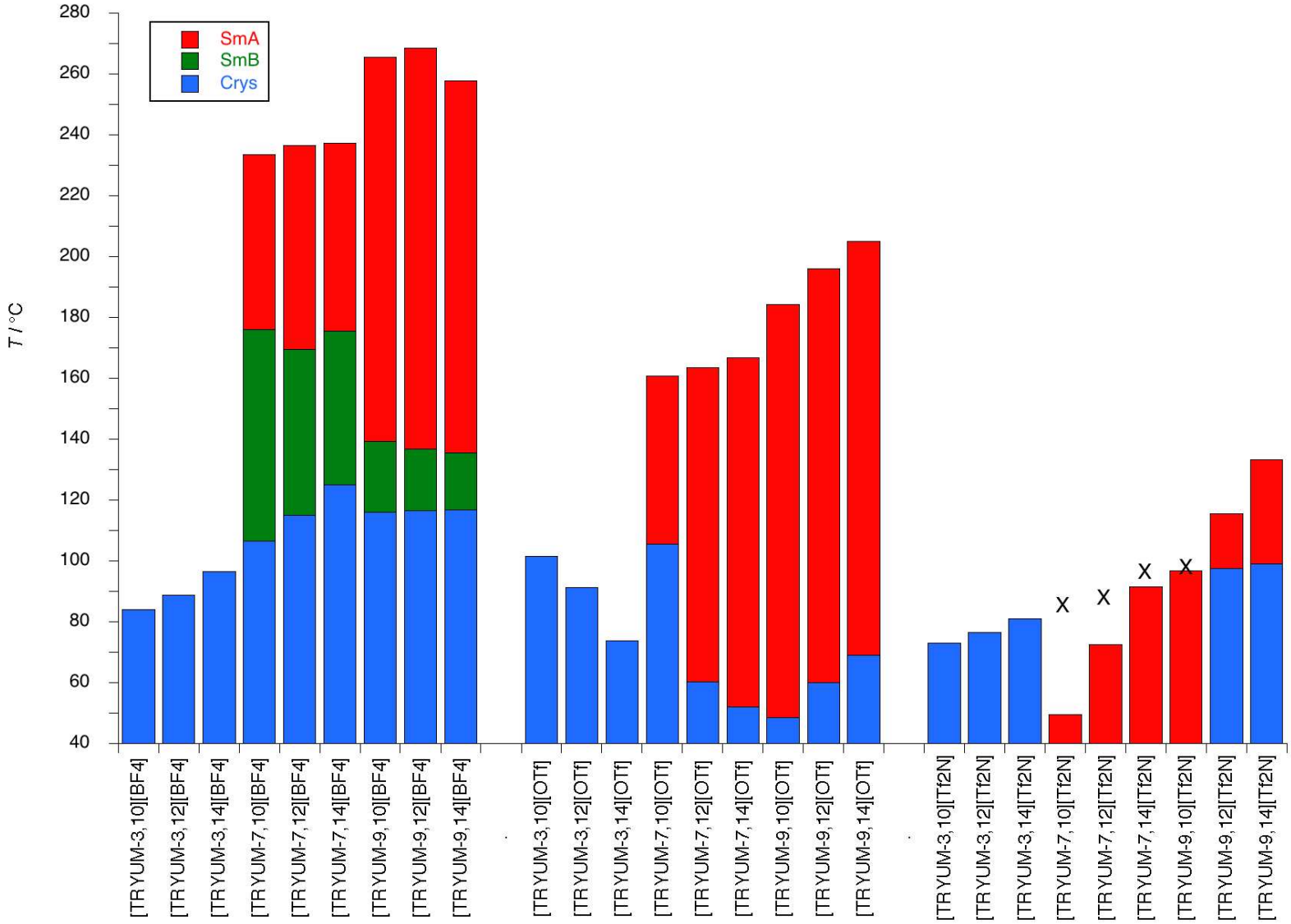

Figure 1. Plot of transition temperatures of the triazolium salts grouped by perfluoroalkyl-chain and anion.
In the data for the Tf_2N salts, the position of 'X' represents the melting point (mesophases are monotropic for these compounds). Data are included for published compounds ([TRYUM-3,*n*][OTf] and [TRYUM-3,*n*][OTf])

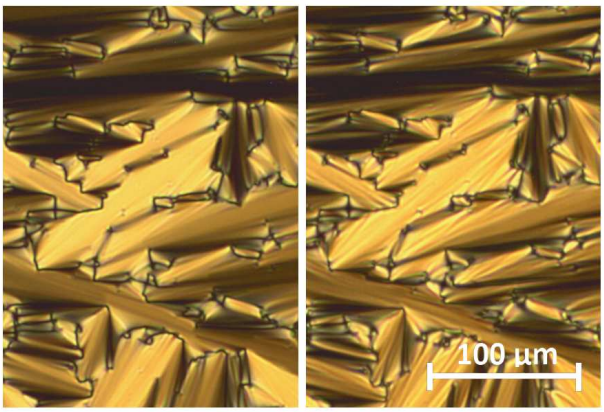

Figure 2. Microphotographs taken on cooling from the isotropic liquid. On the left, compound **[TRYUM-7,10][BF_4]** at 183.3 °C in SmA phase and the same sample at 152.5 °C in SmB on the right.

Considering the materials that do show liquid crystal phases, in general the clearing points are related inversely to the size of the anion, which is in turn related to its charge dispersion. Thus, the most stable phases are seen with BF_4^- (smallest and least charge disperse) and the least stable with Tf_2N^- (largest and most charge disperse). Interestingly, there is little variation in clearing enthalpy (Figure S19) across the three series of salts and the clearing entropy (which normalises for temperature) also shows relatively little variation although the values for the BF_4^- salts are slightly smaller (DSC data are found in the ESI, section 3). Chain length has little influence on clearing points for the BF_4^- salts or **[TRYUM-7,*n*][OTf]**, while for the Tf_2N^- salts and **[TRYUM-9,*n*][OTf]**, the effect is stronger. Melting points increase with chain length where the anion is BF_4^-, Tf_2N^- and **[TRYUM-9,*n*][OTf]**, but decrease for **[TRYUM-3,*n*][OTf]** and **[TRYUM-7,*n*][OTf]**. Given the rather short core (phenyltriazolium), it is not unsurprising that the salts with the short perfluoropropyl chain are not mesomorphic.

Small-angle Scattering

In order to derive information about the organisation in the mesophases, the compounds were studied by small-angle X-ray scattering (SAXS) and small-angle neutron scattering (SANS). There was very good agreement between the SAXS and SANS data and so the former are discussed here, while the latter are found in the SI. In the SmA phase, the complexes typically showed a (001) reflection from the smectic layers as well as a weaker (002) reflection (Figure 3a) showing the

reasonably well-developed layering on account of the electrostatic forces binding the layers together. In addition, there is a broad reflection at *ca* 16° 2θ which corresponds to the side-to-side separation of the perfluorinated chains in the smectic layers. In the tetrafluoroborate salts, there is also a SmB phase (Figure 3b) and the additional order reveals a (003) lamellar reflection as well as an in-layer (010) reflection and a slightly sharper reflection associated with the perfluorinated chains consistent with the greater degree of order compared to the SmA phase.

A complete set of data for the compounds is found in Table S2 and its consideration is interesting. The length of a **[TRYUM-7,10]**$^+$ cation in the all-*trans* configuration of the chains is estimated to be 30 Å from the X-ray single-crystal structure.[75] However, the SAXS data show that the layer spacing is appreciably larger, with some dependence on the anion (Figure 4). Thus, for Tf_2N salts, the layer spacing is just over 30% greater than the cation length, while it is *ca* 50% greater for OTf and *ca* 60% greater for BF_4. These increases are the signature of a bilayer structure, which have arisen because of the amphiphilicity of the cations bearing a hydrocarbon chain at one end and a fluorocarbon chain at the other. For example, compound **7a** (Figure 5) shows a SmC phase with a layer spacing of 36.9 Å, whereas the analogue **7b** with a semiperfluoro chain at one end also shows a SmC phase, but this time with a layer spacing of 76.4 Å, the doubling arising from the mutual association of the hydrocarbon chains and of the fluorocarbon chains. In the present case, the fact that the phase is orthogonal and that the layer spacing is always less than twice the cation length points either to chain folding/kinking, interdigitation or some mix of the two. The fact that the spacing depends on anion size, with the greatest spacing found with the smallest anion (BF_4^-) is consistent with at least some interdigitation. Thus, the larger the anion, the greater the potential cation···cation separation, creating free volume into which a chain may penetrate. As the volume of the fluorocarbon chains is about 50% greater than that of the hydrocarbon chain and as the former are quite rigid, then interdigitation (or chain folding) is likely to be associated with the hydrocarbon chain.

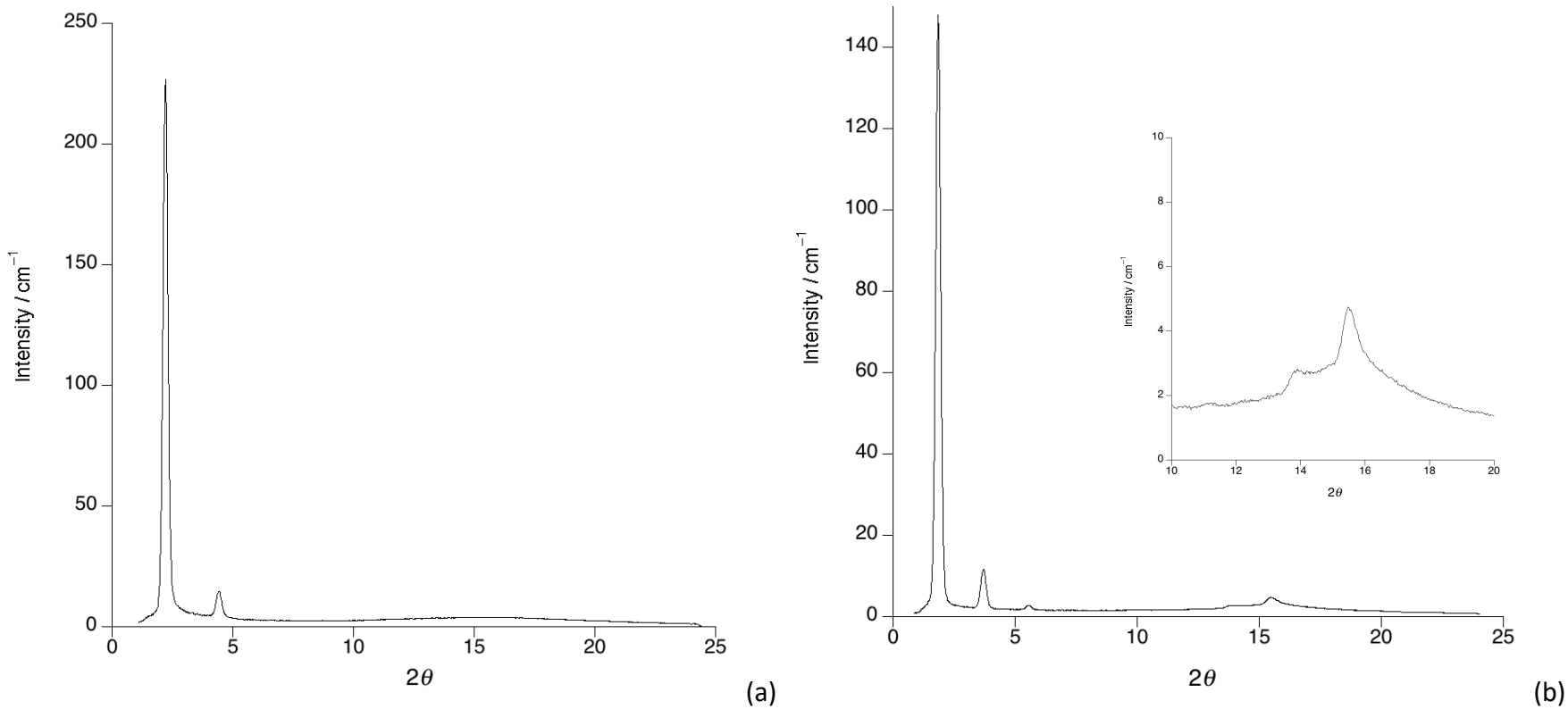

Figure 3. SAXS pattern for (a) SmA phase of [TYRUM-7,10][Tf_2N] at 45 °C and (b) SmB phase of [TYRUM-7,10][BF_4] at 158 °C – inset shows the wide-angle region and the (010) reflection at $2\theta \approx 14°$.

In addition to studying the liquid crystal phases, it can be instructive to examine the isotropic phase of ionic liquids, as it is common to find residual short-range order at different lengthscales, namely the so-called polar non-polar peak, PNPP, charge ordering peak, COP, and contact peak, CP,[87,88] which can provide extra information (Figure S19).

The contact peak (CP) and charge-ordering peak (COP), found at mid to wide angles in the SAXS experiment, arise from, respectively, the cation-anion separation (4.5-5.0 Å) and the distance between two cations of like charge (8 Å). The polar/non-polar peak (PNPP), found normally at small angles, typically represents a bilayer structure akin to a 'fragment' of SmA phase and in effect quantifies the separation of cations by flexible alkyl chains, as found in many 'common' ILs, such as those based on 1-alkyl-3-methylimidazolium ions.[87] Data collected in the isotropic phase of the various salts (except for some BF_4^- salts where decomposition was an issue) showed broadly two types of scattering pattern. All show a contact peak (CP) at wider angles around 5 Å and while Figure 6b shows some possible hint of a COP, the data were not good enough to allow reliable deconvolution. The **[TRYUM-*m*,10][Tf_2N]**, salts with *m* = 7 and 9 show a low-angle reflection (Figure 6a) that is partially resolved into two components, whereas consideration of Figure 6b, recorded for **[TRYUM-3,10][Tf_2N]**, appears to show a single but somewhat broader peak. The breadth of the peak for **[TRYUM-3,10][Tf_2N]** could mean that it is formed of two reflections close in value and indeed fitting the data shows that it can be deconvoluted into two signals using a model comprising two Lorentz peaks. Thus, Figure 7 shows the low-angle reflection for **[TRYUM-7,10][Tf_2N]** in the isotropic state illustrating the need for a two-peak model to fit the data. Fitting parameters are reported in Table S3 (ESI).

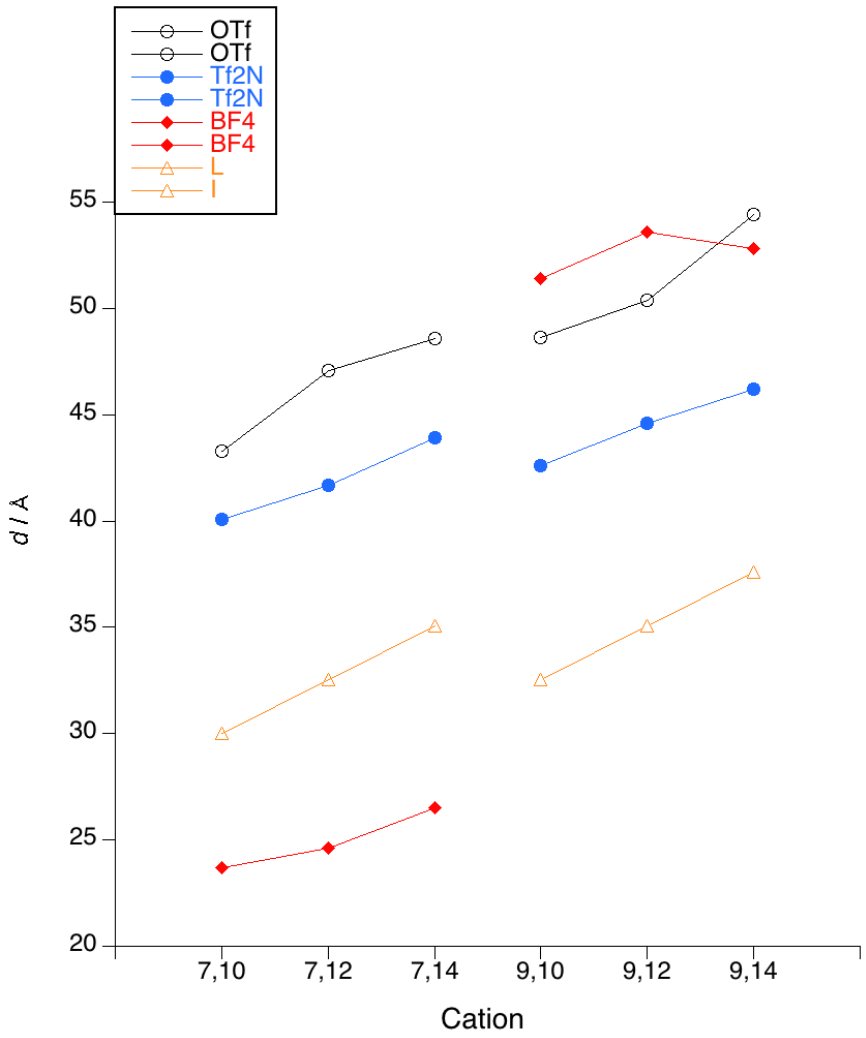

Figure 4. Plot showing the measured layer spacings from SAXS data for the compounds under study.

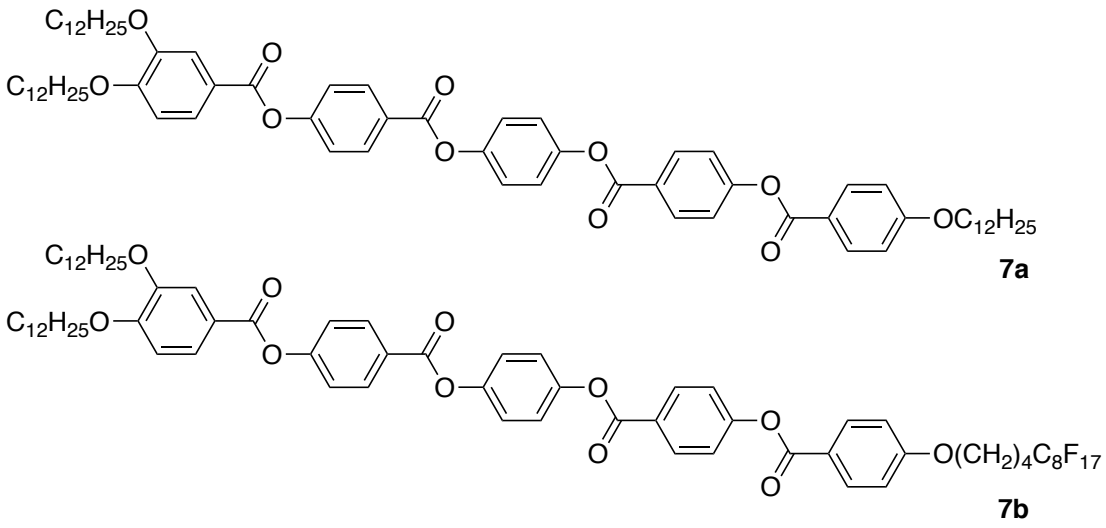

Figure 5. Tricatenar liquid crystals without (**7a**) and with (**7b**) a semiperfluorocarbon chain.

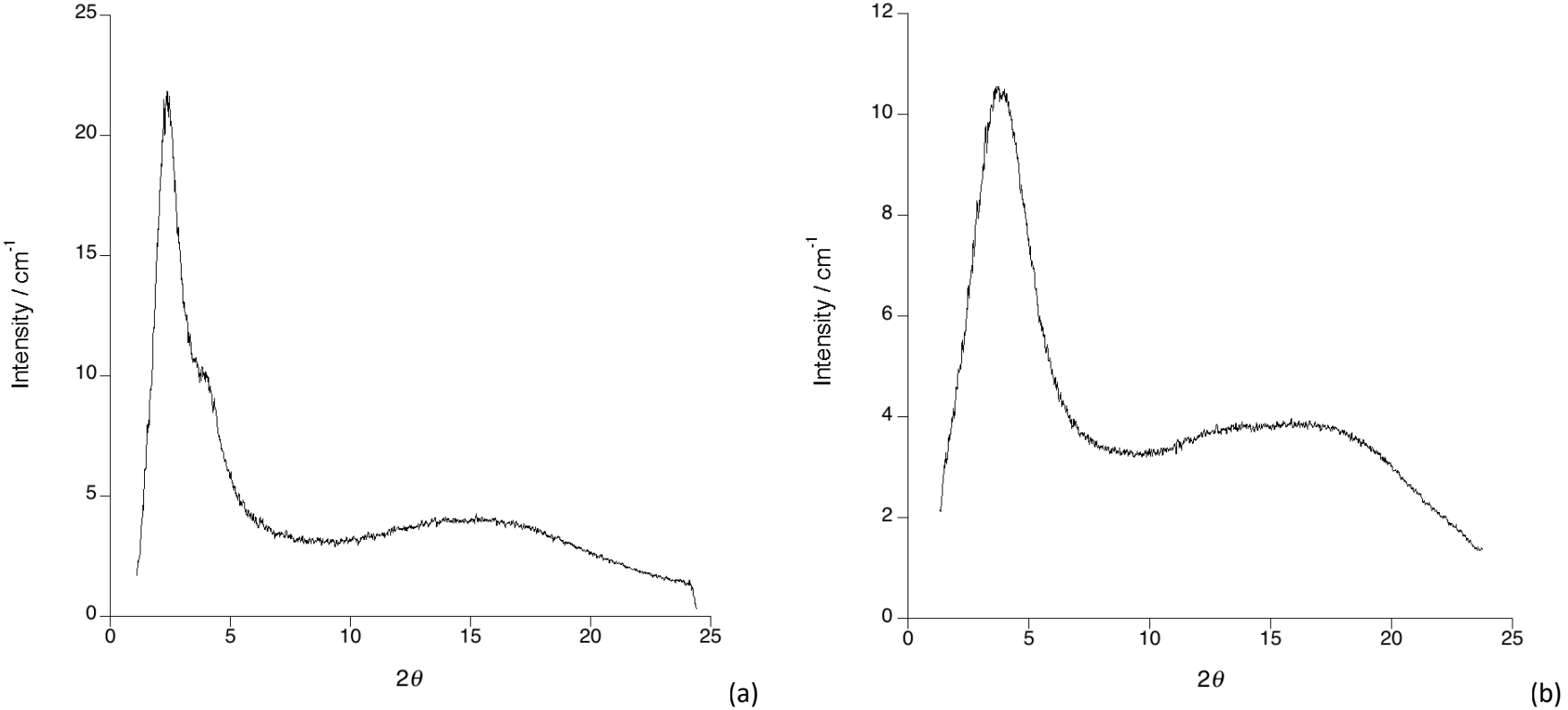

Figure 6. SAXS pattern in the isotropic phase for (a) **[TRYUM-7,10][Tf_2N]** at 89 °C and (b) **[TRYUM-3,10][Tf_2N]** at 78 °C.

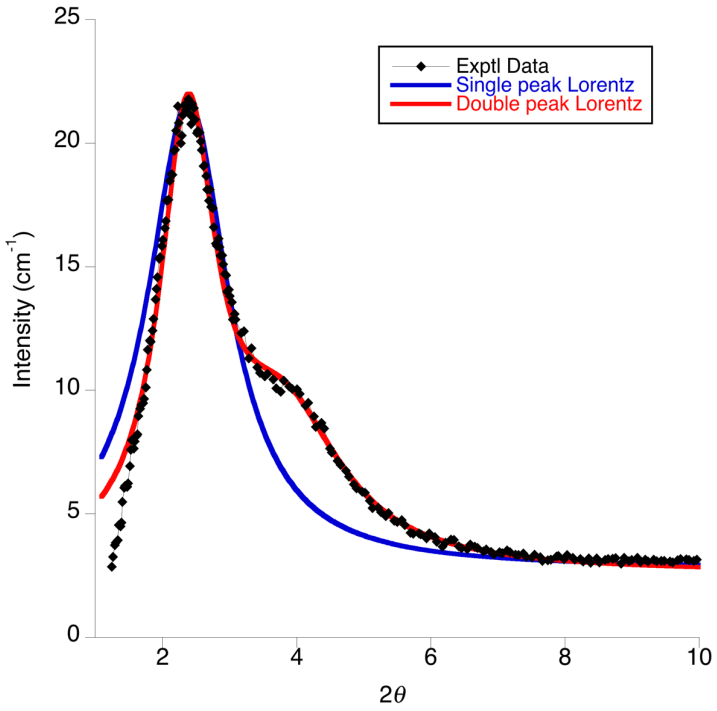

Figure 7. Comparison between the single and double peak models fit to SAXS data recorded on **[TRYUM-7,10][Tf_2N]** in isotropic liquid.

The results of the fitting are plotted in Figure 8 which shows the evolution of the two reflections as a function of both alkyl and perfluoroalkyl chain length, and also of anion. The pattern of the data is the same for each anion, in that there is an evolution of the value for both reflections as a function of the alkyl chain length, but the difference between the two values is actually fairly constant as a function of the perfluoroalkyl chain length. In fact, evaluation of the difference shows a fairly close correspondence with the length of the perfluoroalkyl chain (estimated readily from the data for **[TRYUM-7,10][OTf]** reported previously[75]). However, while the values for the smaller-angle reflection of the two scale with both the alkyl and perfluoroalkyl chain lengths and correlate well with the cation length, the other scales only with the alkyl chain length and is independent of the perfluoroalkyl chain length. This suggests that, according to the original meaning of a PNPP as noted earlier, then the wider-angle reflection of the two corresponds to the separation of cations by alkyl chains and so is properly the PNPP. Considering then the general incompatibility between hydrocarbon and perfluorocarbon chains, it is reasonable to assume that there is a bilayer structure with short-range correlations that respects this preferred separation. This is illustrated schematically in Figure 9.

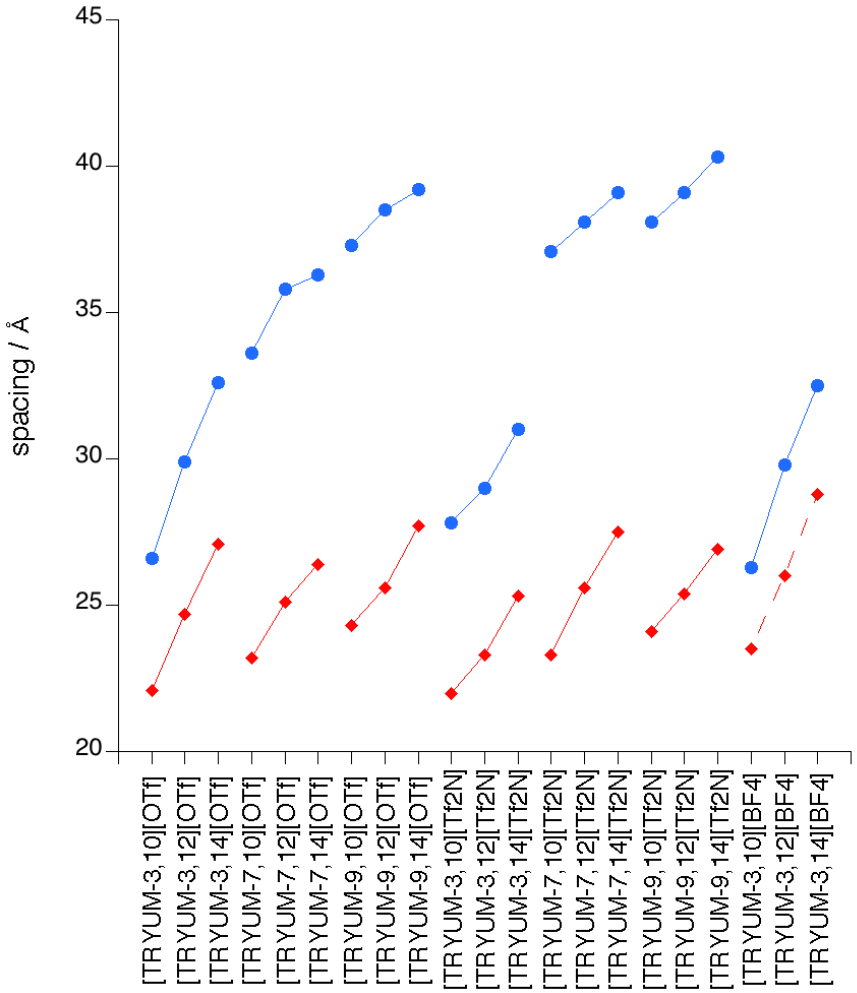

Figure 8. Spacing data from SAXS in the isotropic phase of the salts. Blue data points represent the PNPP and red data points the PNPP'.

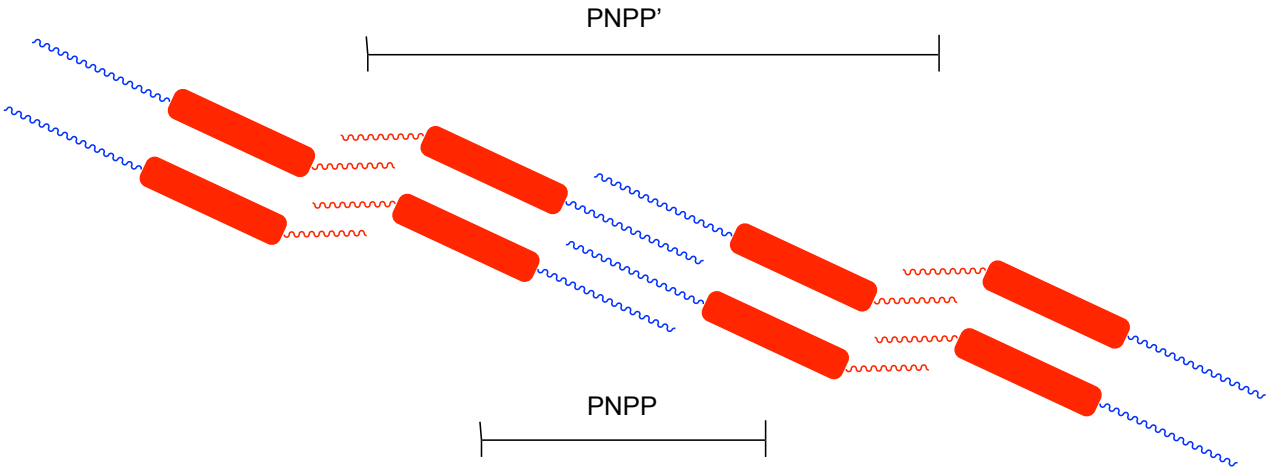

Figure 9. Proposed local structure for the TRYUM salts in the isotropic liquid showing the origin of the PNPP and PNPP’ periodicities Note that there is only short-range correlation.

Figure 9 then shows the origin of the smaller-angle component of the peak as reflecting the effective length of a bilayer structure arising from the hydrocarbon/fluorocarbon chain immiscibility. The separation is labelled PNPP' and it is evident from the schematic figure why this would scale with the fluorocarbon chain length as observed. In the same way that the PNPP reflects a 'fragment' of SmA phase, so the PNPP' would reflect a fragment of a bilayer SmA_2 phase. The exceptions are the data derived from the BF_4^- salts where the differences between the PNPP and PNPP' are smaller than the length of the C_3F_7– chain. The origin of the difference is systematically due to the value of the PNPP and may therefore arise from the fitting of the data.

Finally here, there is, however, one very curious feature found in a number of tetrafluoroborate. Thus, on entering the SmA phase from the isotropic liquid, a sharp reflection is observed in the small-angle region at around $2\theta = 3.9°$ (example for **[TRYUM-7,10][BF_4]**) with a much weaker, broad reflection at smaller angle (Figure 10). As the sample is cooled further, the lower-angle peak grows in intensity and sharpens, in many cases becoming the stronger of the two low-angle reflections, which then have a relationship (in terms of spacing) as (001) and (002) reflections, corresponding to *d*-spacings of 47.4 and 22.9 Å, respectively. Interestingly, this (002) spacing corresponds to the PNPP spacing for the same cation, which we have attributed to the length of the core plus alkoxy chain of the cation (it is shorter than the total length of the cation, which is around 30 Å if an all-*trans* arrangement of the alkyl chains is assumed). What this suggests is that the bilayer structure proposed for the isotropic phase exists also in the SmA phase at lower temperatures with the same origin, namely the mutual incompatibility of alkyl and perfluoroalkyl chains. The proposal then is that the incompatibility can be overcome thermally and so is not well-defined at higher temperatures, implying an analogy with consolution temperatures, although here the effect would appear to occur over a temperature range rather than at a critical temperature. The monolayer structure, observed at higher temperature, presumably appears as the length of the hydrocarbon portion of the cation due to the separation of the polar parts of the molecules by the alkyl chains and the difference in scattering length density between the chains and polar domains.

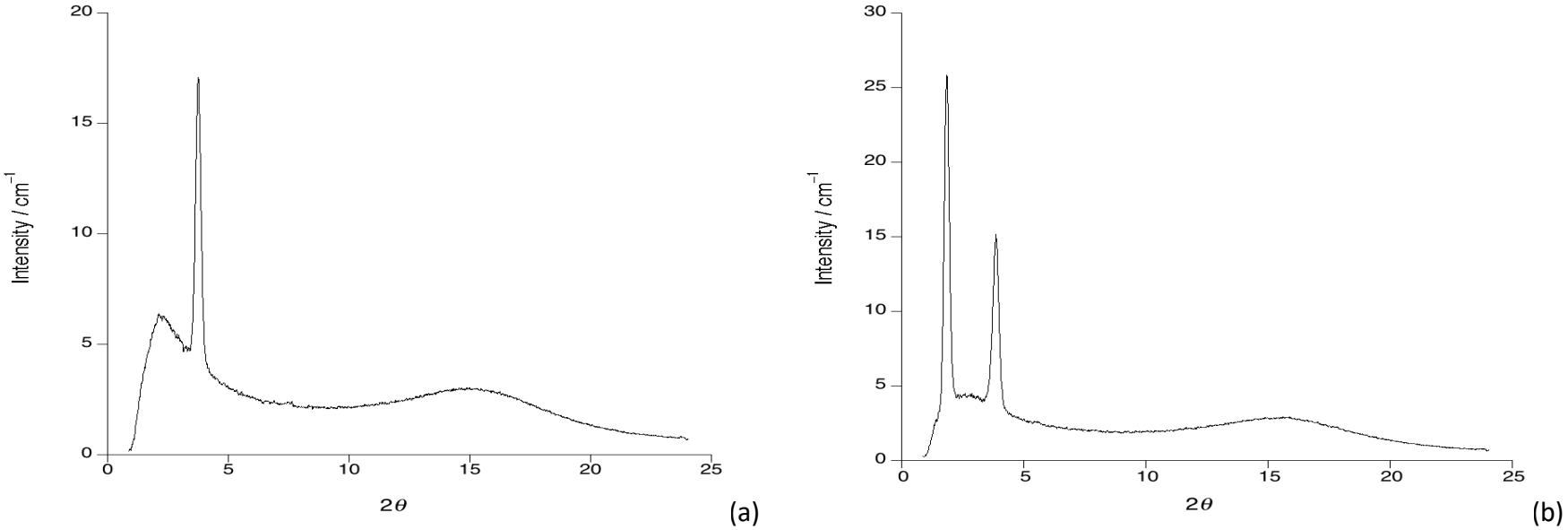

Figure 10. SAXS patterns for **[TRYUM-7,10][BF_4]** at (a) 150 °C and (b) 110 °C.

Electrochemical Impedance Spectroscopy

Due to the interest in ILs and ILCs as electrolytes and therefore to understand the ion mobility of these materials,[89] conductivities were determined using Electrochemical Impedance Spectroscopy (EIS) measurements in a bespoke, high-temperature cell.[90–92] Samples were analysed in the liquid crystal and/or isotropic phases over a range of temperatures, collecting four or five data points in each phase. Conductivities were then extracted by fitting the EIS data to a suitable equivalent circuit model (see ESI for details). Conductivity data and fitting parameters, when the temperature-dependent conductivity data were fitted to Arrhenius and Vogel-Fulcher-Tammann (VFT) models, are reported in Table S4 in the ESI. Figure 11 shows a plot of conductivity as a function of temperature.

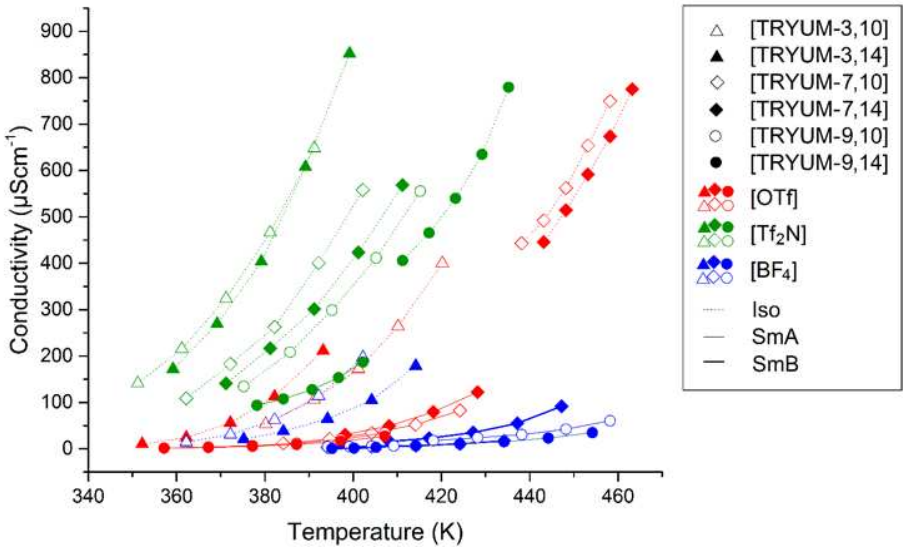

Figure 11. A plot of triazolium salt conductivities as function of temperature.

The data clearly show that the highest conductivities, in all phases, are exhibited by the Tf_2N^- salts, followed by the OTf^- and then the BF_4^- salts. This is consistent with the lower observed viscosities for Tf_2N^- salts and the greater charge delocalisation in the anion, which reduces the strength of anion−cation interactions allowing higher ion mobility,[91] even if this is presumably offset to some extent by the size of this anion.

Similar arguments would then readily account for the relative conductivities of the OTf^- and BF_4^- salts. As expected, conductivities are higher in the isotropic liquids than the ILC phases, reflecting the reduced ion mobility induced by the anisotropic ordering in the liquid crystal phases. Cation-dependent trends in these data are more complex to interpret, due to the range of temperatures spanned by the data, but in general, increasing the length of the alkyl chain leads to a reduction in conductivity, consistent with an increase in the molecular volume[93] of the cation. A similar effect is seen with increasing fluoroalkyl chain length, but this is more pronounced, potentially reflecting the greater rigidity of the fluoroalkyl chains or greater localised ordering.

While the triazolium salts presented here show relatively low conductivity values compared with materials commonly used in opto-electric devices such as dye-sensitised solar cells,[94–96] they do offer the prospect of anisotropic conductivity[84,97], which is something that is yet to be exploited in such materials.

Conclusions

This comprehensive study has led to a range of interesting observations. The materials described can properly be regarded as triphilic on account of the hydro- and fluoro-carbon chains as well as the electrostatic charge on the triazolium ring. That the liquid crystal phase behaviour is dominated by the ionic nature of these materials is shown by the prevalence of the SmA phase, as is common in many ILCs. It is also interesting to note that the bistriflimide salts also show this phase. Thus, despite its size, when in conjunction with a large cation, it is clear that Tf_2N^- does not suppress mesophase formation. The hydrocarbon/ fluorocarbon immiscibility of the cations reveals itself in the observation, using SAXS, of lamellar periodicities that are appreciably greater than the length of a single cation with all-*trans* hydrocarbon chains, pointing to a bilayer structure. However, the measured layer spacings are less than those required for a true bilayer, pointing to a degree of interdigitation or folding of the hydrocarbon chains (smaller in volume than the fluorocarbon equivalents), the extent of which increases with the size of the anion.

SAXS data in the isotropic phase of the materials show that short-range associations of lamellar fragments are maintained, but, interestingly, the appearance of two longer-range correlations (assigned as PNPP and PNPP') provide evidence for local associations that respect the triphilic nature of the materials even in the isotropic phase. Conductivity data are consistent with observed viscosities and mirror a qualitative view of the cation-anion interaction, as reflected in the anion charge dispersity, greatest for Tf_2N^- and least for BF_4^-. Thus, this scaffold has shown how the self-organisation and physical properties in the mesophases of these triphilic materials may be influenced by their molecular composition.

Experimental

For experimental details refer to the Supporting Information.

Conflicts of interest

There are no conflicts to declare.

Acknowledgements

AR thanks the Università Degli Studi di Palermo and the University of York for financial support, the STFC for a grant (RB1710406) for materials and beam time on SANS2D and Dr Jordan Herod for help in collecting the neutron data.

References

1 J. Sherwood, J.H. Clark, I.J.S. Fairlamb, J.M. Slattery, *Green Chem.* 2019, **21**, 2164–2213.

2 J. Li, S. Yang, W. Wu, H. Jiang, *Eur. J. Org. Chem.* 2018, 1284–1306.

3 R.L. Vekariya, *J. Mol. Liq.* 2017, **227**, 44–60.

4 H.P. Steinrück, P. Wasserscheid, *Catal. Lett.*. 2015, **145**, 380–397.

5 Q. Zhang, S. Zhang, Y. Deng, *Green Chem.* 2011, **1***3*, 2619–2637.

6 J.P. Hallett, T. Welton, *Chem. Rev.* 2011, **111**, 3508–3576.

7 V.I. Pârvulescu, C. Hardacre, *Chem. Rev.* 2007, **107**, 2615–2665.

8 R. Giernoth, in: J. Bargon, L.T. Kuhn (Eds.), *Top. Curr. Chem. Collect. B. Ser.*, 2007: pp. 1–23.

9 T. Welton, *Coord. Chem. Rev.* 2004, **248**, 2459–2477.

10 M. Abai, M.P. Atkins, A. Hassan, J.D. Holbrey, Y. Kuah, P. Nockemann, A.A. Oliferenko, N. V. Plechkova, S. Rafeen, A.A. Rahman, R. Ramli, S.M. Shariff, K.R. Seddon, G. Srinivasan, Y. Zou, *Dalton Trans.* 2015, **44**, 8617–8624.

11 E. Jónsson, *Energy Storage Mater.* 2020, **25**, 827–835.

12 L. Yu, G.Z. Chen, *Front. Chem.* 2019, **7**, 1–15.

13 C. Zhong, Y. Deng, W. Hu, J. Qiao, L. Zhang, J. Zhang, *Chem. Soc. Rev.* 2015, **44**, 7484–7539.

14 Y. Zhao, T. Bostrom, *Curr. Org. Chem.* 2015, **19**, 556–566.

15 J. Wu, Z. Lan, J. Lin, M. Huang, Y. Huang, L. Fan, G. Luo, *Chem. Rev.* 2015, **115**, 2136–2173.

16 G.G. Eshetu, M. Armand, B. Scrosati, S. Passerini, *Angew. Chem. - Int. Ed.* 2014, **53**, 13342–13359.

17 J.F. Wishart, *Energy Environ. Sci.* 2009, **s**, 956–961.

18 M. Armand, F. Endres, D.R. Mac Farlane, H. Ohno, B. Scrosati, *Mater. Sustain. Energy.,* 2010, 129–137.

19 L. Yin, S. Li, X. Liu, T. Yan, *Sci. China Mater.* 2019, **62**, 1537–1555.

20 H. Ohno, M. Yoshizawa-Fujita, Y. Kohno, *Bull. Chem. Soc. Jpn.* 2019, **92**, 852–868.

21 K. Matsumoto, J. Hwang, S. Kaushik, C.Y. Chen, R. Hagiwara, *Energy Environ. Sci.* 2019, **12**, 3247–3287.

22 H. Liu, H. Yu, *J. Mater. Sci. Technol.* 2019, **35,** 674–686.

23 M. Forsyth, L. Porcarelli, X. Wang, N. Goujon, D. Mecerreyes, *Acc. Chem. Res.* 2019, **52**, 686–694.

24 Q. Yang, Z. Zhang, X.G. Sun, Y.S. Hu, H. Xing, S. Dai, *Chem. Soc. Rev.* 2018, **47**, 2020–2064.

25 G.Z. Chen, *Int. Mater. Rev.* 2017, **62,** 173–202.

26 A. Balducci, in: *Top. Curr. Chem. Collect. B. Ser.*, 2017: pp. 1–27.

27 S. Wegner, C. Janiak, in: *Top. Curr. Chem. Collect. B. Ser*., 2017: pp. 153–184.

28 K.L. Luska, P. Migowski, W. Leitner, *Green Chem.* 2015, **17**, 3195–3206.

29 J.D. Scholten, B.C. Leal, J. Dupont, *ACS Catal. 2012*, **2**, 184–200.

30 T. Torimoto, T. Tsuda, K.I. Okazaki, S. Kuwabata, *Adv. Mater.* 2010, **22**, 1196–1221.

31 Z. Li, Z. Jia, Y. Luan, T. Mu, *Curr. Opin. Solid State Mater. Sci.* 2008, **12,** 1–8.

32 M. Antonietti, D. Kuang, B. Smarsly, Y. Zhou, *Angew. Chem. - Int. Ed.* 2004, **43**, 4988–4992.

33 M. Aghaie, N. Rezaei, S. Zendehboudi, *Renew. Sustain. Energy Rev.* 2018, **96**, 502–525.

34 G. Cui, J. Wang, S. Zhang, *Chem. Soc. Rev.* 2016, **45**, 4307–4339.

35 X. Zhang, X. Zhang, H. Dong, Z. Zhao, S. Zhang, Y. Huang, *Energy Environ. Sci.* 2012, **5**, 6668–6681.

36 M. Ramdin, T.W. De Loos, T.J.H. Vlugt, *Ind. Eng. Chem. Res.* 2012, **51**, 8149–8177.

37 P. Wasserscheid, T. Welton, *Ionic Liquids in Synthesis*, Wiley-VCH Verlag GmbH & Co. KGaA, Weinheim, Germany, 2007.

38 A. Marciniak, *Int. J. Mol. Sci.* 2010, **11**, 1973–90.

39 K. Binnemans, *Chem. Rev.* 2005, **105**, 4148–4204.

40 K. Goossens, K. Lava, C.W. Bielawski, K. Binnemans, *Chem. Rev.* 2016, **116,** 4643–4807.

41 I. Dierking, *Textures of Liquid Crystals*, Wiley-VCH Verlag GmbH & Co. KGaA, Weinheim, FRG, 2003.

42 K. V. Axenov, S. Laschat, *Materials (Basel).* 2011, **4**, 206–259.

43 Y. Gao, J.M. Slattery, D.W. Bruce, *New J. Chem. 2011*, **35,** 2910–2918.

44 M. Yoshio, T. Kagata, K. Hoshino, T. Mukai, H. Ohno, T. Kato, *J. Am. Chem. Soc.* 2006, **128**, 5570–5577.

45 A. Safavi, M. Tohidi, *J. Phys. Chem. C.* 2010, **114,** 6132–6140.

46 N. V. Shvedene, O.A. Avramenko, V.E. Baulin, L. G. Tomilova, I. V. Pletnev, *Electroanalysis*. 2011, **23**, 1067–1072.

47 M. Yoshio, T. Ichikawa, H. Shimura, T. Kagata, A. Hamasaki, T. Mukai, H. Ohno, T. Kato, *Bull. Chem. Soc. Jpn.* 2007, **80**, 1836–1841.

48 M. Henmi, K. Nakatsuji, T. Ichikawa, H. Tomioka, T. Sakamoto, M. Yoshio, T. Kato, *Adv. Mater.* 2012, **24**, 2238–2241.

49 T. Ito, S. Otobe, T. Oda, T. Kojima, S. Ono, M. Watanabe, Y. Kiyota, T. Misawa, S. Koguchi, M. Higuchi, M. Kawano, Y. Nagase, *Polymers (Basel).* 2017, **9**, 1–14.

50 T.D. Do, A.R. Schmitzer, *RSC Adv.* 2015, **5**, 635–639.

51 Y. Yang, R.I. Boysen, J. Chowdhury, A. Alam, M.T.W. Hearn, *Anal. Chim. Acta*. 2015, **872**, 84–94.

52 D.W. Bruce, Y. Gao, J.N. Canongia Lopes, K. Shimizu, J.M. Slattery, *Chem. – Eur. J.* 2016, **22**, 16113–16123.

53 K. Goossens, P. Nockemann, K. Driesen, B. Goderis, C. Görller-Walrand, K. Van Hecke, L. Van Meervelt, E. Pouzet, K. Binnemans, T. Cardinaels, *Chem. Mater.* 2008, **20,** 157–168.

54 J. Baudoux, P. Judeinstein, D. Cahard, J.C. Plaquevent, *Tetrahedron Lett.* 2005, **4***6*, 1137–1140.

55 C.J. Bowlas, D.W. Bruce, K.R. Seddon, *Chem. Commun.* 1996, 1625–1626.

56 J.D. Holbrey, K.R. Seddon, *J. Chem. Soc. Dalton Trans.* 1999, 2133–2139.

57 V. Busico, P. Corradini, M. Vacatello, *J. Phys. Chem.* 1982, *86*, 1033–1034.

58 V. Busico, P. Cernicchlaro, P. Corradini, M. Vacatello, *J. Phys. Chem.* 1983, **87**, 1631–1635.

59 K. Goossens, K. Lava, P. Nockemann, K. Van Hecke, L. Van Meervelt, P. Pattison, K. Binnemans, T. Cardinaels, *Langmuir*. 2009, **25**, 5881–5897.

60 A. Beneduci, S. Cospito, M. La Deda, L. Veltri, G. Chidichimo, *Nat. Commun.* 2014, **5**, 1–8.

61 T. Li, F. Xu, W. Shi, *Chem. Phys. Lett.* 2015, **628**, 9–15.

62 A.A. Fernandez, L.T. de Haan, P.H.J. Kouwer, *J. Mater. Chem. A*. 2013, **1**, 354–357.

63 A.E. Bradley, C. Hardacre, J.D. Holbrey, S. Johnston, S.E.J. McMath, M. Nieuwenhuyzen, *Chem. Mater.* 2002, **14**, 629–635.

64 M. Hird, *Chem. Soc. Rev.* 2007, **36,** 2070–2095.

65 C. Tschierske, *Top. Curr. Chem.* 2012, **318**, 1–108.

66 D. Almantariotis, T. Gefflaut, A.A.H. Pádua, J.-Y. Coxam, M.F.C. Gomes, *J. Phys. Chem. B*. 2010, **114**, 3608–3617.

67 C.G. Piscopo, F. Trapani, A. Polyzoidis, M. Schwarzer, A. Pace, S. Löbbecke, *New J. Chem.* 2016, **40**, 8220–8224.

68 F. Lo Celso, I. Pibiri, A. Triolo, R. Triolo, A. Pace, S. Buscemi, N. Vivona, *J. Mater. Chem.* 2007, **17**, 1201–1208.

69 I. Pibiri, A. Pace, S. Buscemi, N. Vivona, L. Malpezzi, *Heterocycles*. 2006, **68**, 307–321.

70 I. Pibiri, A. Pace, S. Buscemi, V. Causin, F. Rastrelli, G. Saielli, *Phys. Chem. Chem. Phys.* 2012, **14**, 14306–14314.

71 A. Abate, A. Petrozza, G. Cavallo, G. Lanzani, F. Matteucci, D.W. Bruce, N. Houbenov, P. Metrangolo, G. Resnati, *J. Mater. Chem. A*. 2013, **1**, 6572–6578.

72 I. Zama, G. Gorni, V. Borzatta, M.C. Cassani, C. Crupi, G. Di Marco, *J. Mol. Liq.* 2016, **223**, 749–753.

73 G. Cavallo, G. Terraneo, A. Monfredini, M. Saccone, A. Priimagi, T. Pilati, G. Resnati, P. Metrangolo, D.W. Bruce, *Angew. Chem. Int. Ed.* 2016, **55**, 6300–6304.

74 S. Pensec, F.-G. Tournilhac, P. Bassoul, C. Durliat, *J. Phys. Chem. B*. 1998, **102,** 52–60.

75 A. Riccobono, R.R. Parker, A.C. Whitwood, J.M. Slattery, D.W. Bruce, I. Pibiri, A. Pace, *Chem. Commun.* 2018, **54**, 9965–9968.

76 K. Stappert, A.-V. Mudring, *RSC Adv.* 2015, **5**, 16886–16896.

77 K. Stappert, D. Uenal, B. Mallick, A.V. Mudring, *J. Mater. Chem. C*. 2014, **2**, 7976–7986.

78 K. Stappert, D. Unal, E.T. Spielberg, A.-V. Mudring, *Cryst. Growth Des.* 2015, **15**, 752–758.

79 S. Buscemi, A. Pace, I. Pibiri, N. Vivona, D. Spinelli, *J. Org. Chem.* 2003, **68**, 605–608.

80 S. Buscemi, A. Pace, I. Pibiri, N. Vivona, C.Z. Lanza, D. Spinelli, *Eur. J. Org. Chem.* 2004, 974–980.

81 A. Pace, S. Buscemi, N. Vivona, *Org. Prep. Proced. Int.* 2005, **37**, 447–506.

82 L.B. Clapp, *Adv. Heterocycl. Chem.* 1976, **20**, 65–116.

83 S. Buscemi, A. Pace, A.P. Piccionello, G. Macaluso, C. Organica, D. Spinelli, G. Giorgi, *J. Mater. Chem.* 2005, **70**, 3288–3291.

84 I. Pibiri, A. Beneduci, M. Carraro, V. Causin, G. Casella, G.A. Corrente, G. Chidichimo, A. Pace, A. Riccobono, G. Saielli, *J. Mater. Chem. C*. 2019, **7**, 7974–7983.

85 G. Casella, V. Causin, F. Rastrelli, G. Saielli, *Liq. Cryst.* 2014, **14**, 1–13.

86 G. Casella, V. Causin, F. Rastrelli, G. Saielli, *Liq. Cryst.* 2016, **43**, 1161–1173.

87 A. Triolo, O. Russina, H.-J. Bleif, E. Di Cola, *J. Phys. Chem. B*. 2007, **111,** 4641–4644.

88 K. Shimizu, C.E.S. Bernardes, J.N. Canongia Lopes, *J. Phys. Chem. B*. 2014, **118**, 567–576.

89 Y. Wang, H. Yang, *Chem. Eng. J.* 2009, **147,** 71–78.

90 M.T. Clough, C.R. Crick, J. Gräsvik, P.A. Hunt, H. Niedermeyer, T. Welton, O.P. Whitaker, *Chem. Sci.* 2015, **6**, 1101–1114.

91 A.J.R. Rennie, V.L. Martins, R.M. Torresi, P.J. Hall, *J. Phys. Chem. C*. 2015, **119,** 23865–23874.

92 J. Katkevics, A. Viksna, A. Zicmanis, G. Vaivars, *Solid State Ionics*. 2011, **188**, 114–117.

93 J.M. Slattery, C. Daguenet, P.J. Dyson, T.J.S. Schubert, I. Krossing, *Angew. Chem. – Int. Ed.* 2007, **46**, 5384–5388.

94 W. Kubo, K. Murakoshi, T. Kitamura, S. Yoshida, M. Haruki, K. Hanabusa, H. Shirai, Y. Wada, S. Yanagida, *J. Phys. Chem. B*. 2001, **105,** 12809–12815.

95 N. Yamanaka, R. Kawano, W. Kubo, N. Masaki, T. Kitamura, Y. Wada, M. Watanabe, S. Yanagida, *J. Phys. Chem. B*. 2007, **111**, 4763–4769.

96 A. Hagfeldt, *Chem. Soc. Rev.* 2011, **110,** 6595–6663.

97 H. Shimura, M. Yoshio, K. Hoshino, T. Mukai, H. Ohno, T. Kato, *J. Am. Chem. Soc.* **2008**, **130**, 1759–1765.